GPS Solut (2014) 18:355–364
DOI 10.1007/s10291-013-0335-7

ORIGINAL ARTICLE

Multifrequency algorithms for precise point positioning: MAP3

B. Moreno Monge · G. Rodríguez-Caderot · M. C. de Lacy

Received: 20 February 2013 / Accepted: 30 June 2013 / Published online: 16 July 2013

Abstract We present the new MAP3 algorithms to perform static precise point positioning (PPP) from multifrequency and multisystem GNSS observations. MAP3 represents a two-step strategy in which the least squares theory is applied twice to estimate smoothed pseudo-distances, initial phase ambiguities, and slant ionospheric delay first, and the absolute receiver position and its clock offset in a second adjustment. Unlike the classic PPP technique, in our new approach, the ionospheric-free linear combination is not used. The combination of signals from different satellite systems is accomplished by taking into account the receiver inter-system bias. MAP3 has been implemented in MATLAB and integrated within a complete PPP software developed on site and named PCube. We test the MAP3 performance numerically and contrast it with other external PPP programs. In general, MAP3 positioning accuracy with low-noise GPS dual-frequency observations is about 2.5 cm in 2-h observation periods, 1 cm in 10 h, and 7 mm after 1 day. This means an improvement in the accuracy in short observation periods of at least 7 mm with respect to the other PPP programs. The MAP3 convergence time is also analyzed and some results obtained from real triple-frequency GPS and GIOVE observations are presented.

B. Moreno Monge (✉) · G. Rodríguez-Caderot
Department Section of Astronomy and Geodesy,
Faculty of Mathematics, University Complutense of Madrid,
Pza. Ciencias, 3, 28040 Madrid, Spain
e-mail: bmorenom@mat.ucm.es

M. C. de Lacy
Department of Cartographic Engineering,
Geodesy and Photogrammetry, University of Jaén,
Paraje Las Lagunillas s/n, 23008 Jaén, Spain

Keywords Precise point positioning · GNSS · Multifrequency algorithms · Complete covariance matrix · Least squares

Introduction

Precise point positioning (PPP) has become widely studied due to its great operational flexibility and its capability to reach decimeter-level accuracy in kinematic positioning and centimeter-level accuracy in static mode (Bisnath and Gao 2007). Millimeter-level accuracy in static positioning can also be achieved with 1-day observation periods (Kouba and Héroux 2001). The classic PPP strategy is based on the ionospheric-free linear combination of dual-frequency observations to remove the slant ionospheric delay, which increases the observations noise about three times. In addition, an initialization period of several minutes is required until the PPP solution reaches a high accuracy.

In recent years, a number of free PPP online services have become available, such as APPS (apps.gdgps.net), GAPS (gaps.gge.unb.ca), CSRS–PPP (www.geod.nrcan.gc.ca), and magicGNSS (magicgnss.gmv.com). APPS was the first PPP online service processing GPS dual-frequency observations and used the JPL precise satellite products. GAPS only supports GPS data while the other two programs perform static and kinematic PPP from GPS and GLONASS observations using precise products provided by the international GNSS service (IGS). Additionally, the Bernese software version 5.0 (Dach et al. 2007) also processes GPS data in a preliminary PPP mode.

Soon more than 100 modernized satellites belonging to GPS, GLONASS, Beidou, and Galileo will become operational and transmit open access signals in at least three different frequencies simultaneously. Currently, three GPS

Block-IIF satellites are already transmitting L1–L2–L5 signals, and the first four Galileo vehicles have recently been put into orbit. Since 2006, the two GIOVE satellites transmit E1–E5–E6 signals, which are representative of the Galileo signal and are tracked by the Galileo experimental sensor stations (GESS) network. The GESS network, in turn, collects GPS and GIOVE observations worldwide to be used by the Galileo processing center (GPC) in the determination of satellite orbits and clocks. GPC products are available to authorized users through the GIOVE Web site along with GIOVE and GESS estimated inter-frequency bias (IFB) and signal quality statistics (www.giove.esa.int, not available for the time being).

As a consequence, the design of new and powerful PPP algorithms able to exploit the many advantages of the new GNSS signals has become essential. Juan et al. (2012) propose the introduction of additional linear combinations of the observables along with precise ionospheric corrections, which also increases the PPP accuracy and reduces its convergence time. An alternative approach might be to avoid the formation of any linear combination, as shown by Schoenemann et al. (2011), who also propose the estimation of uncalibrated phase delays in the process, thus reducing the convergence time and improving the repeatability of the PPP solution (Ge et al. 2006, 2008). However, it is still difficult to quantify the potential improvements arising from the introduction of multifrequency data in the PPP process, due to the limited number of satellites currently transmitting multifrequency signals.

In this context, the MAP3 algorithms have been developed to perform static PPP with the future multisystem and multifrequency GNSS constellation. MAP3 represents a two-step strategy in which the least squares (LS) theory is exploited to estimate smoothed pseudo-distances, initial phase ambiguities, and slant ionospheric delay in a first step, and the receiver position and its clock offset in a second adjustment. Unlike the classic PPP technique, MAP3 avoids the ionospheric-free linear combination, thus broadening PPP to all available frequencies. The integration of different satellite systems is accomplished by considering the receiver inter-system bias (ISB), which can be either eliminated with precise known values or estimated as an additional parameter. Complete covariance matrices accounting for temporal correlations are formed and used within the process, giving rise to a more realistic stochastic model. Additionally, the estimation of the ionospheric delay constitutes a valuable source of information to detect disturbances, which can severely degrade the positioning, as shown in Moreno et al. (2011). MAP3 has been implemented in MATLAB and integrated within a complete PPP software developed on site and named PCube. This program contains all models and corrections required in the PPP process to estimate the receiver position at the millimeter-level accuracy by means of two different approaches, a sequential filter and MAP3.

The MAP3 algorithms are introduced and tested with real GPS dual-frequency observations, their convergence in time is analyzed, and some results obtained from real triple-frequency GPS and GIOVE observations are presented.

Design of the algorithms

MAP3 consists of two main parts. As shown in Fig. 1, MAP3-1 processes undifferenced code and phase multifrequency observations separately for each observed satellite and provides estimations of smoothed pseudo-distances, initial phase ambiguities, and slant ionospheric delay. Then, MAP3-2 combines the estimated pseudo-distances for all observed satellites in a second LS adjustment to recover the receiver position and its clock offset. Additional products, such as corrections to the tropospheric zenith wet delay (ZWD) and the receiver ISB, may also be estimated by MAP3-2.

Module MAP3-1: smoothed pseudo-distances, initial phase ambiguities, and ionospheric delay estimation

The mathematical model of Euler and Goad (1991) for the GPS observables is applied here in a multifrequency context by taking into account all possible errors and effects in the observations,

$$\begin{aligned} P_i(t) &= \rho(t) + k_{1i} I_1(t) + v_{P_i} \\ L_i(t) &= \rho(t) - k_{1i} I_1(t) + \beta_i + v_{L_i} \end{aligned} \tag{1}$$

where $i = 1, 2, 3, \ldots$, P_i and L_i are the undifferenced code and phase observations, respectively, expressed in distance units. The pseudo-distances $\rho(t)$ are formed by grouping the geometric distance $R(t)$, the receiver and satellite clock

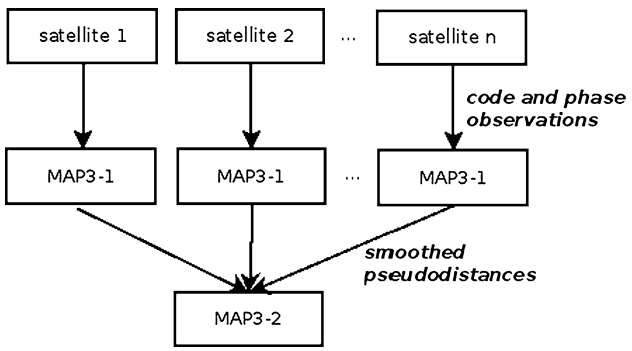

Fig. 1 Scheme of MAP3

offsets $dt_r(t)$ and $dt^s(t)$, and the tropospheric error $T(t)$, i.e., $\rho(t) = R(t) + c(dt_r(t) - dt^s(t)) + T(t)$, and c being the speed of light. The ionospheric delay at frequency f_1 is denoted by $I_1(t)$ and is multiplied by the coefficient $k_{1i} = f_1^2/f_i^2$, depending on the frequencies. The initial phase ambiguities are $\beta_i = L_{0i} + \lambda_i N_i$, where the initial phases are denoted by L_{0i}, the initial integer ambiguities are N_i, and λ_i are the wave lengths. Finally, v_{P_i} and v_{L_i} represent the code and phase ranges noise, respectively, including thermal noise, receiver, and satellite multipath.

The expressions (1) are biased by the satellite and receiver electronic hardware delays, which are rather stable in time and can be considered constant for short periods of time. We will not deal here with the correction of phase electronic delays, since they are absorbed by the ambiguities estimation. The code electronic delays, however, may be corrected by using the differential code bias (DCB) provided by the center for orbit determination in Europe (CODE) in the way proposed in ICD-GPS-200 (2000). In our previous analysis, it was observed that both, the accurate estimation of the ionospheric delay and the processing of GIOVE observations, require the correction of GPS code delays and GIOVE IFB.For the sake of simplicity, we will focus hereafter on the triple-frequency case, although the expressions used can be easily adapted to any number of frequencies. Thus, the mathematical model expressed in matrix form is (De Lacy et al. 2008)

$$\begin{aligned} \mathbf{P}(t) &= A_1\boldsymbol{\xi}(t) + \boldsymbol{v}_P \\ \mathbf{L}(t) &= A_2\boldsymbol{\xi}(t) + \boldsymbol{\beta} + \boldsymbol{v}_L \end{aligned} \tag{2}$$

where $\mathbf{P} = (P_1(t), P_2(t), P_3(t))^T$, $\mathbf{L} = (L_1(t), L_2(t), L_3(t))^T$, $\boldsymbol{\xi}(t) = (\rho(t), I_1(t))^T$, $\boldsymbol{\beta} = (\beta_1, \beta_2, \beta_3)^T$, $A_1 = \begin{pmatrix} 1 & 1 \\ 1 & k_{12} \\ 1 & k_{13} \end{pmatrix}$, and $A_2 = \begin{pmatrix} 1 & -1 \\ 1 & -k_{12} \\ 1 & -k_{13} \end{pmatrix}$.

For an observation period of n_t epochs, the design matrix of a LS approach is written as

$$A = \begin{pmatrix} A_1 & & & 0 \\ A_2 & & & U_3 \\ & A_1 & & 0 \\ & A_2 & & U_3 \\ & & \ddots & \vdots \\ & & A_1 & 0 \\ & & A_2 & U_3 \end{pmatrix} \tag{3}$$

with U_3 being the three-dimensional unit matrix. The observation vector is formed by grouping $\mathbf{P}(t)$ and $\mathbf{L}(t)$ for $t = 1, \ldots, n_t$, and the vector of unknowns by grouping $\boldsymbol{\xi}(t)$, with $t = 1, \ldots, n_t$, and $\boldsymbol{\beta}$. It must be stressed that the initial phase ambiguities are assumed to remain constant during the whole observation period, and consequently, the phase observations must be free from cycle slips.

The stochastic model used in MAP3-1 is formed by a diagonal matrix Q, whose diagonal elements Q_P and Q_L contain the observations formal noise, about 20 cm for code and 2 mm for phase ranges, divided by the square cosine of the satellite zenith angle at each observation epoch.

As shown in De Lacy et al. (2008), the LS theory provides explicit expressions for the estimation of the parameters

$$\begin{aligned} \hat{\beta} = &\left(D^{-1} - Q_L D^{-1} Q_L^{-1} A_2 N^{-1} A_2^T Q_L^{-1}\right)\bar{\mathbf{L}} \\ &- Q_L D^{-1} Q_L^{-1} A_2 N^{-1} A_1^T Q_P^{-1}\bar{\mathbf{P}} \end{aligned} \tag{4}$$

and

$$\begin{aligned} \hat{\xi}(t) = &N^{-1} A_2^T D^{-1} Q_L^{-1} A_2 N^{-1}\left(A_1^T Q_P^{-1}\bar{\mathbf{P}} + A_2^T Q_L^{-1}\bar{\mathbf{L}}\right) \\ &+ N^{-1}\left(A_1^T Q_P^{-1}\mathbf{P}(t) + A_2^T Q_L^{-1}\mathbf{L}(t)\right) - N^{-1} A_2^T Q_L^{-1} D^{-1}\bar{\mathbf{L}} \end{aligned} \tag{5}$$

where $\bar{\mathbf{P}}$ and $\bar{\mathbf{L}}$ denote the arithmetic mean of code and phase observations along the complete observation period, $N = A_1^T Q_P^{-1} A_1 + A_2^T Q_L^{-1} A_2$ and $D = \left(U_3 - A_2 N^{-1} A_2^T Q_L^{-1}\right)$. These expressions are formed by small matrices of dimension 3, thereby reducing significantly the computational time and memory usage. The covariance matrices of the estimated parameters are

$$C_{\hat{\beta}\hat{\beta}} = \hat{\sigma}_0^2 \frac{1}{n_t} D^{-1} Q_L \tag{6}$$

and

$$C_{\hat{\xi}(t)\hat{\xi}(t)} = \hat{\sigma}_0^2 \left(N^{-1} + \frac{1}{n_t} N^{-1} A_2^T D^{-1} Q_L^{-1} A_2 N^{-1}\right) \tag{7}$$

where $\hat{\sigma}_0^2$ is the a posteriori variance.

Module MAP3-2: receiver position and clock offset estimation

The smoothed pseudo-distances estimated with MAP3-1 for all observed satellites may be combined in a second LS adjustment to recover the receiver position and its clock offset. The mathematical model used this time for all satellites in view $s = 1, \ldots, n_s$ is

$$\tilde{\rho}^s(t) = R^s(t) + c(\mathrm{d}t_r(t) - \mathrm{d}t^s(t)) + T(t) + v \tag{8}$$

where $\tilde{\rho}^s(t)$ denotes the smoothed pseudo-distance previously estimated, $R^s(t)$ is the geometric distance (X^s, Y^s, Z^s), and (X, Y, Z) are the satellite and receiver Cartesian coordinates, respectively. At this point, precise satellite orbits and clocks must be used and the tropospheric delay may be approximated by means of a model (Saastamoinen 1973;

Hopfield 1972), although a correction to the ZWD must also be estimated at least every 2 h. Finally, v denotes the smoothed pseudo-distances noise, which is at a few millimeter level.

Considering an observation period of n_t epochs and linearizing (8) using a set of a priori receiver coordinates $\mathbf{X}_0$, the mathematical model can be written as

$$\begin{pmatrix} U_{n_t} & \tilde{G}^1 & M_w^1 \\ U_{n_t} & \tilde{G}^2 & M_w^2 \\ \vdots & \vdots & \vdots \\ U_{n_t} & \tilde{G}^{n_s} & M_w^{n_s} \end{pmatrix} \begin{pmatrix} c\,\mathbf{dt}_r \\ \delta X \\ \delta Y \\ \delta Z \\ \mathbf{ZWD} \end{pmatrix} - \begin{pmatrix} \mathbf{y}^1 \\ \mathbf{y}^2 \\ \vdots \\ \mathbf{y}^{n_s} \end{pmatrix} = \begin{pmatrix} \mathbf{v}^1 \\ \mathbf{v}^2 \\ \vdots \\ \mathbf{v}^{n_s} \end{pmatrix} \tag{9}$$

where U_{n_t} is the n_t-dimensional unit matrix, the matrices $\tilde{G}^s$ are formed by the direction cosines between the receiver and the satellite s at each observation epoch, and the matrices M_w^s contain the mapping functions for the estimation of a correction to the tropospheric ZWD every 2 h. For the sake of simplicity, the matrices $\tilde{G}^s$ and M_w^s are grouped in $G^s = \begin{pmatrix} \tilde{G}^s & M_w^s \end{pmatrix}$. The vector of unknowns is formed by the receiver clock offset at every observation epoch in meters $c\,\mathbf{dt}_r$, corrections to the a priori receiver position $(\delta X,\ \delta Y,\ \delta Z)$, and a correction to the tropospheric wet delay for every 2-h period, **ZWD**. The observation vector consists of the smoothed pseudo-distances corrected with a priori ranges, precise satellite clock offsets and the tropospheric delay given by a nominal model, i.e., for each satellite s

$$\mathbf{y}^s = \begin{pmatrix} \tilde{\rho}^s(t_1) - R_0^s(t_1) + c\,dt^s(t_1) - T^s(t_1) \\ \tilde{\rho}^s(t_2) - R_0^s(t_2) + c\,dt^s(t_2) - T^s(t_2) \\ \vdots \\ \tilde{\rho}^s(t_{n_t}) - R_0^s(t_{n_t}) + c\,dt^s(t_{n_t}) - T^s(t_{n_t}) \end{pmatrix} \tag{10}$$

Finally, $\mathbf{v}^s$ contains the residuals of the adjustment for the satellite s. The stochastic model used in MAP3-2 is given by the block matrix $C_{\mathbf{yy}}$, where every block in the diagonal, $C_{\mathbf{y^s y^s}}$, is obtained from the covariance matrix of the smoothed pseudo-distances. More specifically, by discarding the ionospheric delay variance and covariance terms in (7), the complete matrix

$$Q_{\mathbf{yy}} = \begin{pmatrix} d+a & a & \cdots & a \\ a & d+a & & \vdots \\ \vdots & & \ddots & a \\ a & \cdots & a & d+a \end{pmatrix} = dU_{n_t} + a\mathbf{e}\mathbf{e}^T \tag{11}$$

is formed, with d being the first element in N^{-1}, a the first element in $N^{-1}A_2^T D^{-1} Q_L^{-1} A_2 N^{-1}$ divided by the number of observations n_t, and $\mathbf{e} = (1,\ 1,\ 1,\ \ldots,\ 1)^T$. The matrices $C_{\mathbf{y^s y^s}}$ are then obtained by multiplying $Q_{\mathbf{yy}}$ by the corresponding a posteriori variance. It is stressed that (11) is a simplification of the covariance matrix, since the ionospheric delay variance terms are discarded. However, this simplification gives a full variance–covariance matrix that includes the temporal correlations and has the inverse

$$Q_{\mathbf{yy}}^{-1} = \frac{1}{d}\left(U_{n_t} - \frac{a}{d + n_t a}\mathbf{e}\mathbf{e}^T\right) \tag{12}$$

Analogously, applying the LS theory and operating with block matrices, the following expressions are obtained

$$\delta\hat{\mathbf{X}} = \begin{pmatrix} \delta\hat{X} \\ \delta\hat{Y} \\ \delta\hat{Z} \\ \hat{\mathbf{ZWD}} \end{pmatrix} = \Delta^T d_1 + \gamma d_2 \tag{13}$$

and

$$c\,\hat{\mathbf{dt}}_r = \Gamma d_1 + \Delta d_2 \tag{14}$$

where $d_1 = \sum_{s=1}^{n_s} C_{\mathbf{y^s y^s}}^{-1}\mathbf{y^s}$, $d_2 = \sum_{s=1}^{n_s} G^{sT} C_{\mathbf{y^s y^s}}^{-1}\mathbf{y^s}$, $\gamma = \left(F - E^T\bar{N}^{-1}E\right)^{-1}$, $\Delta = -\bar{N}^{-1}E\gamma$, $\Gamma = \bar{N}^{-1}\left(U_{n_t} - E\Delta^T\right)$, $\bar{N} = \sum_{s=1}^{n_s} C_{\mathbf{y^s y^s}}^{-1}$, $E = \sum_{s=1}^{n_s} C_{\mathbf{y^s y^s}}^{-1} G^s$, and $F = \sum_{s=1}^{n_s} G^{sT} C_{\mathbf{y^s y^s}}^{-1} G^s$. The covariance matrices of the estimated parameters are

$$\begin{aligned} C_{\delta\hat{\mathbf{X}}\delta\hat{\mathbf{X}}} &= \hat{\sigma}^2\gamma \\ C_{\hat{\mathbf{dt}}_r\hat{\mathbf{dt}}_r} &= \hat{\sigma}^2\Gamma \end{aligned} \tag{15}$$

where $\hat{\sigma}^{\cdot 2}$ is the a posteriori variance of the second LS adjustment.The combination of observations from different satellite systems can be accomplished only by taking into account the ISB introduced by the receiver circuitries. The ISB can be eliminated with precise values given by the corresponding analysis centers (GPC, IGS) or estimated with MAP3-2 as an additional time delay between the observations.

Implementation of MAP3

PCube is a flexible software that processes GPS and Galileo/GIOVE observations and supports IGS and GPC precise products as well as navigation message. The combination of IGS and GPC products can be accomplished by taking into account the corresponding time offsets (Píriz et al. 2008).

As illustrated in Fig. 2, PCube is structured in various modules. The input only consists of an observation file in Rinex 2.xx or 3.00 format. The processing options must also be set up. Then, the module "m_Extractor" automatically downloads the products needed during the process [satellite products, earth orientation parameters (EOP) and

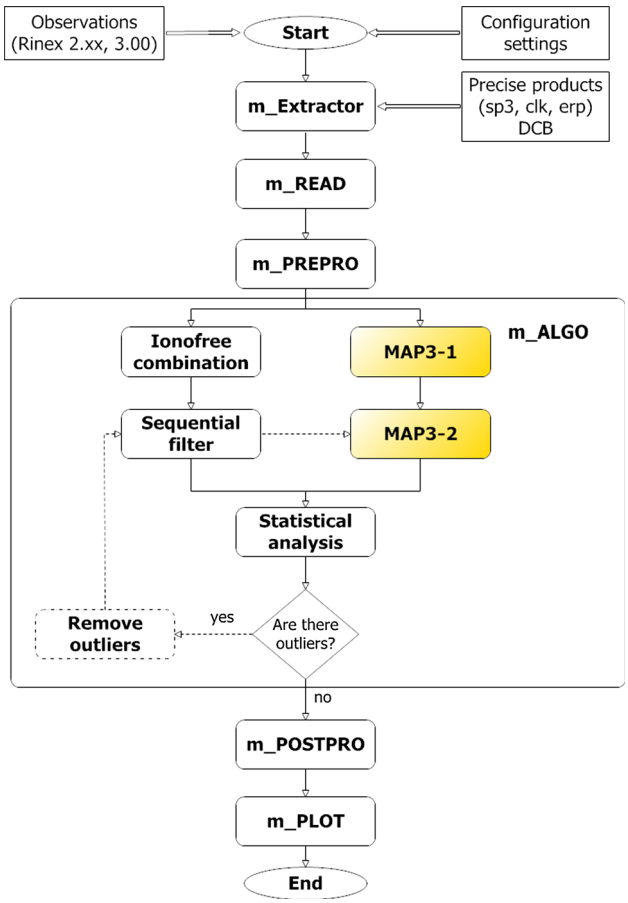

Fig. 2 PCube software flowchart

DCB] from the corresponding servers. Next, the module "m_READ" reads the observation and product files and stores the information in different MATLAB structures. The "m_PREPRO" module performs the preprocessing of the observations in various steps, carrying out the detection of outliers and cycle slips following the techniques described in Dach et al. (2007), interpolates the satellite orbits and clocks to the observation epochs, and applies the correction of relativistic effects, tropospheric delay, antennas phase center offset and variations (PCO/V), electronic delays, and phase wind-up (Wu et al. 1993). Then, "m_ALGO" estimates the receiver position by means of two different strategies: a sequential filter applied to the ionospheric-free linear combination of dual-frequency observations, as described in Kouba and Héroux (2001), and the MAP3 algorithms. In the same module, the residuals are analyzed by means of statistical tests until no outliers are detected among the observations. Next, "m_POSTPRO" completes the corrections to the estimated position due to the antenna height, earth and pole tides, and ocean loading (Petit and Luzum 2010), and hence, PCube mathematical model is sufficient for positioning accuracy at the millimeter level. Finally, the results are plotted by the "m_PLOT" module. A set of auxiliary functions are grouped in the called "m" module and additional directories are used to store observation and product files, structures, and figures.

Numerical tests of MAP3

In order to evaluate the performance of the MAP3 algorithms, a series of numerical tests were carried out with real GPS dual-frequency observations. The results are compared with other PPP programs. In particular, the online services CSRS-PPP, magicGNSS, and APPS, the sequential filter implemented in PCube, and the software Bernese 5.0 are used. Since the convergence time of the PPP solution is a critical issue, the MAP3 convergence time is characterized here by analyzing the accuracy reached in periods of increasing length from 2 to 24 h.

In the following tests, the IGS precise orbits and clocks are used (Dow et al. 2009), absolute IGS05 antenna PCO/V corrections are applied, the tropospheric delay is approximated with the Hopfield (1972) model, and a correction to the ZWD is estimated every 2 h. The electronic code delays are corrected by using monthly P1-P2 DCB, and a cutoff elevation angle of 10° is imposed since it provides the most accurate results in combination with a satellite elevation weighting scheme.

Data description

A set of real GPS dual-frequency observations collected at the IGS station USN3 from April 20 to May 10, 2010 (DoY 110–130) was selected. The USN3 station was chosen because it is connected to the H-Maser defined as the primary realization of UTC (USNO), and a stable clock behavior and good data quality are expected. In fact, the estimated noise of the USN3 observations is about 15 cm for the P code.

MAP3 positioning in short observation periods

The performance of MAP3 in short observation periods is evaluated by processing a set of 2-h observation files. The positioning errors are then computed as the difference between the estimated position and the station precise coordinates.

In Fig. 3, the positioning errors obtained with MAP3 and the rest of PPP programs in 2-h observation periods are shown. In most of the days, the accuracy achieved with MAP3 is better than 2 cm and only in a few cases, the errors reach up to 4 cm in the east and up components. The

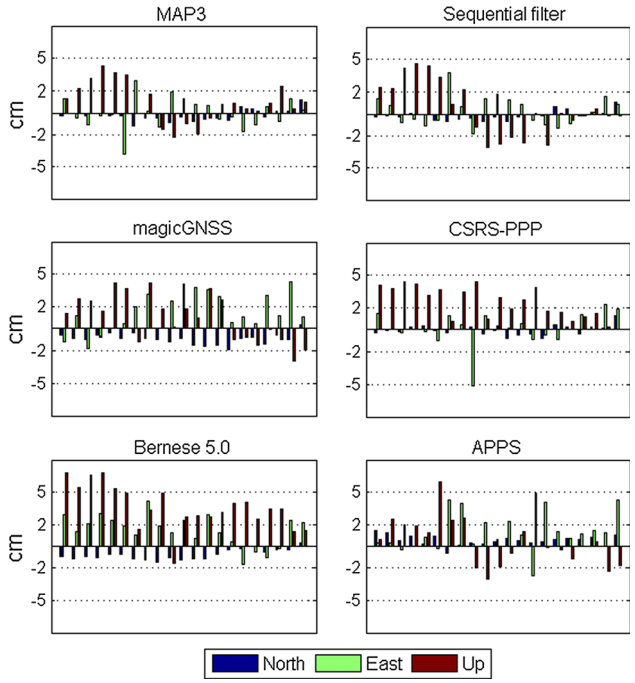

Fig. 3 Short observation period (2 h) positioning error with MAP3 and other PPP programs in north, east, and up

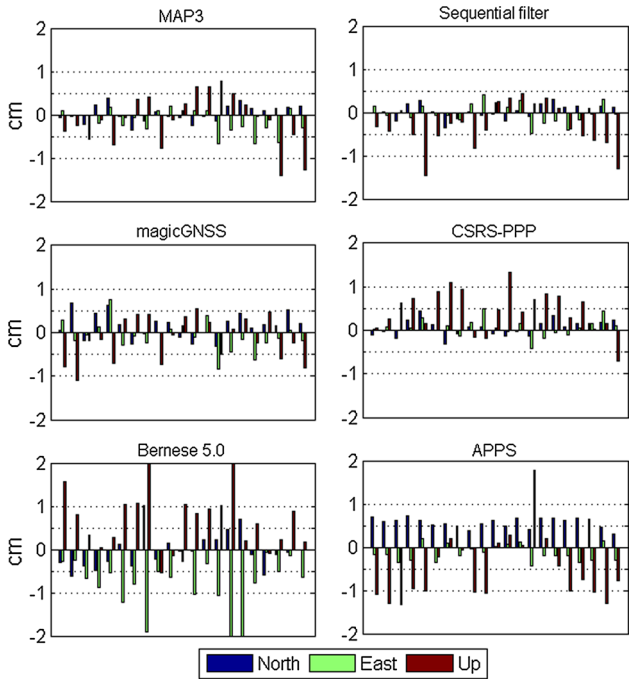

Fig. 4 Long observation periods (24 h) positioning error with MAP3 and other programs in north, east, and up

Table 1 Short observation periods (2 h) positioning results in north, east, up, and 3D

Program	N	E	U	3D
MAP3	0.6	1.4	2.0	2.5
Seq. filter	0.5	1.4	2.4	2.8
CSRS-PPP	0.4	1.5	2.8	3.2
MagicGNSS	1.0	2.3	2.3	3.4
APPS	0.7	2.1	2.4	3.3
Bernese 5.0	1.0	2.0	4.1	4.7

The units are cm

Table 2 MAP3, long observation periods (24 h) positioning results in north, east, up, and 3D

Program	N	E	U	3D
MAP3	0.20	0.31	0.60	0.70
Seq. filter	0.16	0.25	0.61	0.68
CSRS-PPP	0.19	0.21	0.66	0.72
MagicGNSS	0.32	0.35	0.52	0.70
APPS	0.58	0.23	0.91	1.10
Bernese 5.0	0.40	1.09	1.67	2.03

The units are cm

results of the sequential filter are very similar, since the models and corrections used in the process are the same in both cases. The positioning errors of magicGNSS and CSRS-PPP are slightly larger, reaching up to 3–4 cm in many cases. Bernese 5.0 errors are more elevated, reaching up to 5–6 cm. APPS provides accuracy below 2 cm in most cases. The RMS of these errors are presented in Table 1 as a measure of the achieved accuracy. In general, MAP3 positioning accuracy is 6 mm in the north direction, 1.4 cm in the east, and 2 cm in the up. The RMS of MAP3 positioning errors in 3D is 2.5 cm. This result is slightly better than that of the filter (2.8 cm) and even more so compared to the estimations obtained with the other PPP programs, with a difference of 7 mm with respect to the next best solution.

MAP3 positioning in long observation periods

MAP3 performance in long observation periods is evaluated by processing a set of daily observation files. The positioning errors obtained with MAP3 and the rest of programs are shown in Fig. 4. Again, MAP3 provides high-accurate estimations, since in most days the positioning error is below 7 mm and only in 2 cases, the errors reach up to 1.4 cm in the up component. Similar accuracies are obtained with the filter, magicGNSS and CSRS-PPP, with most of the positioning errors below 7 mm. The programs Bernese 5.0 and APPS provide less accurate estimations, with errors around 1 cm in many cases. It must be mentioned that, for the time being, it is recommended to use the Bernese PPP solution only as a priori position (Dach et al.

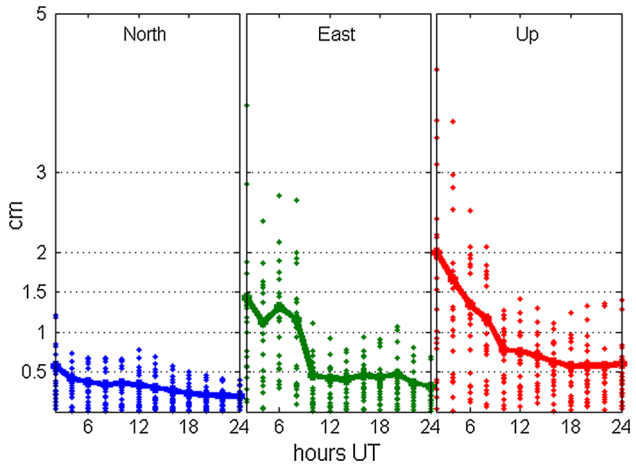

Fig. 5 MAP3 positioning convergence time in north, east, and up

2007). The RMS of the positioning errors are presented in Table 2. In general, MAP3 accuracy in long observation periods is about 2 mm in the north, 3 mm in the east, and 6 mm in the up. The RMS of MAP3 positioning errors in 3D is 7 mm. This result is at the same level of accuracy as reached by the sequential filter and the online programs CSRS-PPP and magicGNSS.

MAP3 convergence time

In order to analyze MAP3 convergence time, a series of observation files increased in steps of 2 h are processed. The positioning errors in the components north, east, and up are shown in Fig. 5. The solid line represents the error RMS obtained in the different observation periods. It can be seen that the north component is estimated at the 5 mm level accuracy from the first 2 h of observations and that the 2 mm level is achieved in 24 h. The east component is about 1.5 cm accurate for the first 2 h, improving significantly to the 5 mm in 10 h and finally reaching 3 mm. The up component is at the 2 cm level accuracy in 2 h, decreasing to 8 mm in 10 h and finally reaching the 6 mm level after 18-h observation. The quick improvement in the accuracy during the first 10 h of observations might be due to the continuous strengthening of the satellite configuration geometry during this period, followed by a slow improvement after 10 h because of the repetition in such configuration, with a period of approximately 12 h for the GPS constellation. Therefore, the combination of different satellite systems, which provides for stronger satellite geometries, should improve the positioning accuracy in the first observation hours and thus reduce MAP3 convergence time.

Positioning in a multifrequency case

Once the performance of MAP3 was confirmed with GPS dual-frequency observations, we decided to apply MAP3 to real GIOVE and GPS triple-frequency data. Although some IGS stations are already tracking the first Galileo signals, these observations are not included in our tests since precise orbits and clocks for the satellites are not yet available.

MAP3 positioning with GIOVE observations

In this test, a set of real GIOVE triple-frequency and GPS dual-frequency observations collected at some stations of the GESS network is processed. The observation period corresponds to the first 2 h of November 1, 2009, when the GIOVE satellites were visible from the stations GVES, GMAL, GWUH, GIEN, and GNNO.

The final GPC orbits and clocks at 5-min sampling rate are used. GPS code delays are corrected by using monthly DCB and GIOVE IFB with values provided by GPC. When observations from both satellite systems are combined in the PPP process, the receiver ISB is estimated. Since only two GIOVE satellites are available, while 7–9 GPS satellites are usually tracked at each epoch, the estimation of the ISB absorbs the common part of the unmodeled errors in the GIOVE observations. Additionally, the receiver clock offset estimation absorbs the residual part of the electronic biases correction. GIOVE antennas PCO are corrected with the values given in Zandbergen and Navarro (2006) and compiled in Table 3. GESS antennas PCO are not corrected since the station coordinates are given for the antenna phase centers. Station and satellite antennas PCV are not considered here, with the concurrent loss of up to a few centimeters in the positioning accuracy. It must be mentioned that some authors have detected large systematic group delay variations and a high multipath in the GESS observations (Crisci et al. 2007; Tobías et al. 2009; De Bakker et al. 2012), which will be reflected in degraded position estimations.

MAP3 positioning is analyzed in two different cases: (1) when GPS-only observations are processed and (2) when GPS and GIOVE observations are combined in the PPP process. Figure 6 shows the positioning errors obtained in these two cases. In general, the errors reach up to 15 cm, probably due to the interpolation of satellite clocks, the lack of PCV corrections, the systematic errors, and the high

Table 3 GIOVE antennas PCO in the *z*-axis direction (Zandbergen and Navarro 2006)

Satellite	PCO *z*-axis (m)
GIOVE-A	0.771
GIOVE-B	1.347

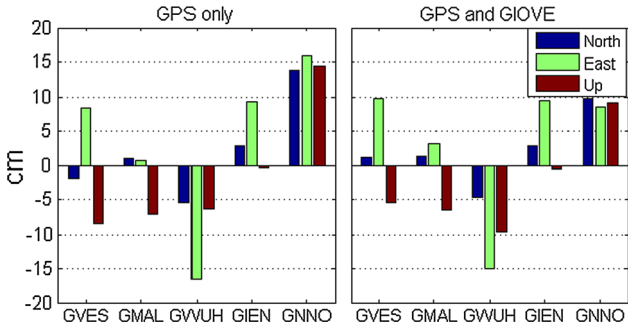

Fig. 6 MAP3 positioning error obtained when processing GESS GPS-only observations (*left*) and GPS + GIOVE observations (*right*) in north, east, and up

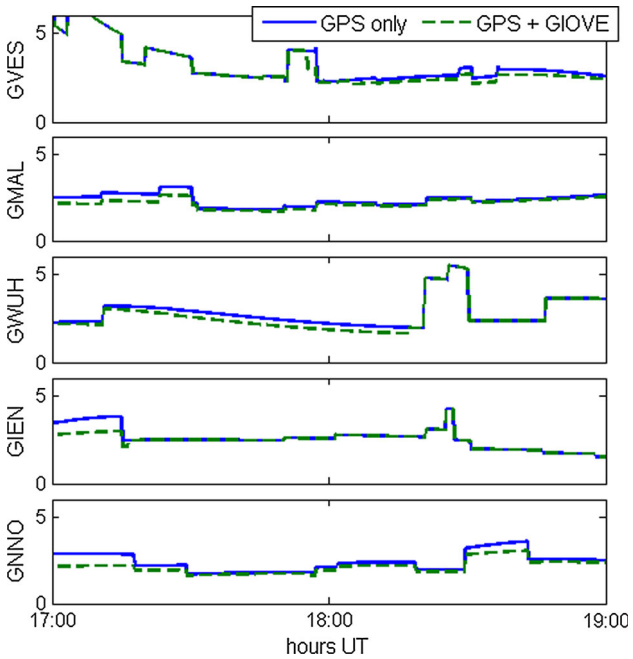

Fig. 7 GDOP when considering GPS-only and GPS + GIOVE signals

multipath detected in the GESS observations. Nevertheless, more accurate estimations are obtained when the GIOVE observations are included in the process, especially for GNNO. The geometric dilution of precision (GDOP) obtained in both cases for the 5 GESS stations is presented in Fig. 7. The improvement in the accuracy observed in most stations is accompanied by a decrease in the GDOP when the two GIOVE satellites are included. The only exception is GIEN, from where the GIOVE satellites were observed only during a short period time. The error degradation observed in the east component in GVES and GMAL might be due to the large multipath detected in the GIOVE observations for these stations (Simsky et al. 2008). The positioning RMS errors obtained in the two cases analyzed are given in Table 4. The introduction of GIOVE observations results in an improvement in the accuracy of almost 2 cm in the north and east components and 1.5 cm in the up with respect to the GPS-only solution. This is a promising result that must be studied better with future Galileo multifrequency observations.

Table 4 MAP3 positioning error RMS in north, east, and up when processing GESS GPS-only and GPS + GIOVE observations

Test	N	E	U
GPS-only	6.84	11.68	8.56
GPS + GIOVE	5.09	9.93	7.00

The units are cm

MAP3 positioning with GPS triple-frequency observations

In a second test, a set of real GPS triple-frequency observations taken at the IGS stations ABMF, BRST, LMMF, ROSA, and ILHA is processed. These stations were chosen because they are tracking the first GPS triple-frequency signals and their IGS precise coordinates are available, which are essential to compare our PPP results. Daily observation files corresponding to August 1–7, 2012 (DoY 214–220) are used in two different processes: (1) when only GPS dual-frequency observations are used and (2) when the observations in the third frequency (L5) from the satellites PRN01 and PRN25 are also included. In recent months, a new modernized GPS satellite was deployed and assigned PRN24, but unfortunately our dataset does not contain its observations.

The final IGS satellite products are used, satellite and receiver antennas PCO/V are corrected by using the IGS08 absolute calibration, and the satellite and receiver DCB are also considered. However, the corresponding corrections for the L5 frequency and station DCB P1C1 are not yet available. Figure 8 shows the positioning errors obtained with MAP3 in both processes. The positioning errors are a few centimeters, probably due to the large code noise in the observations and the lack of station DCB. For the time being, the introduction of the new L5 frequency does not improve PPP accuracy but, on the contrary, it increases the error in the estimations due to the lack of PCO/V and DCB corrections for this frequency. The error increase is especially significant in BRST (1.3 cm in the east), ROSA (3 mm in the up), and ILHA (6 mm in the east); however, in the last case, it is compensated by an improvement of the same magnitude in the up component.

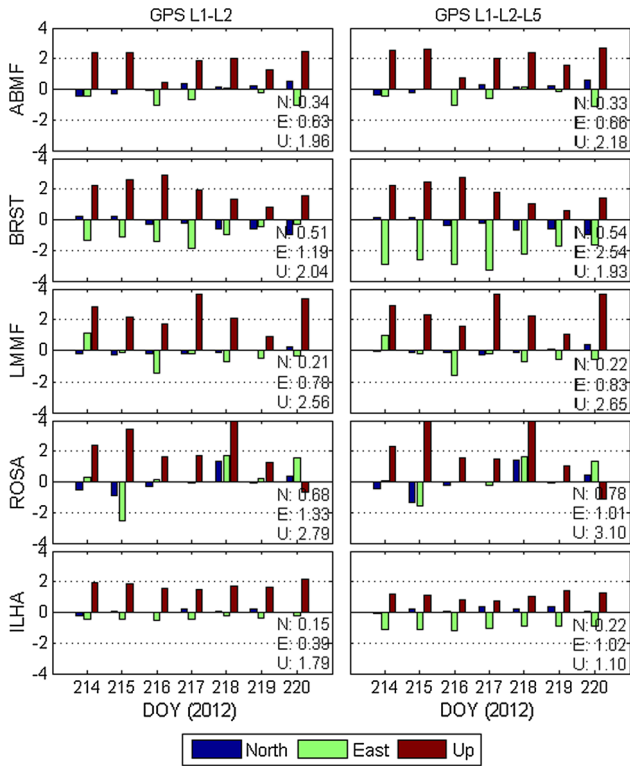

Fig. 8 MAP3 positioning error obtained when processing IGS GPS dual-frequency observations (*left*) and triple-frequency observations (*right*) in north, east, and up. The units are cm. The RMS of the errors are shown within each graphic

Summary and conclusions

The new MAP3 algorithms to perform static PPP from multifrequency and multisystem GNSS observations are presented. The major advantages of the new approach with respect to the classic PPP technique arise from its flexibility to combine multifrequency observations from different satellite systems, without any limitation in the number of frequencies. MAP3 is a two-step strategy in which the LS theory is used to estimate smoothed pseudo-distances, initial phase ambiguities, and slant ionospheric delay in a first step, and the receiver position and its clock offset in a second adjustment. Complete covariance matrices accounting for temporal correlations are formed and used, obtaining a more realistic stochastic model. Additionally, the estimation of ionospheric delay at every epoch provides a valuable source of information to detect ionospheric disturbances.

The numerical tests accomplished here demonstrate that, with low-noise GPS dual-frequency data, MAP3 positioning accuracy is about 2.5 cm after 2 h of observation, 1 cm in 10 h, and 7 mm after 1 day. These results are similar to those obtained with a sequential filter implemented in PCube and improve the achievements of other PPP programs in at least 7 mm in short observation periods (2 h). Similar results are obtained with MAP3, the sequential filter, and the online programs CSRS-PPP and magicGNSS in long observation periods (24 h).

A quick improvement in MAP3 positioning accuracy is observed during the first 10 h of observation, due to the strengthening of the satellite configuration geometry during this period. It is followed by a slow improvement in the accuracy during the next hours, given the repetition of the satellite configuration with a period of about 12 h for the GPS constellation. Thus, the integration of different satellite systems in the PPP process, which will provide for stronger satellite geometries, should improve the positioning accuracy in the first observation hours and reduce MAP3 convergence time.

The tests performed with real GIOVE triple-frequency observations reveal a significant improvement in the positioning accuracy when the GIOVE satellites are included in the PPP process, which is accompanied by a decrease in the GDOP. These promising results must still be confirmed with the future Galileo multifrequency observations.

It is also demonstrated that, for the time being, the introduction in the PPP process of the new GPS L5 signal, already transmitted by the satellites PRN01 and PRN25, degrades the PPP accuracy with respect to the dual-frequency case, due to the lack of antenna offsets and electronic delay corrections for this frequency. In some cases, the error increase is significant, reaching up to 1.3 cm.

Acknowledgments The research was supported by the research projects New Algorithms for the Future Multifrequency GNSS System (Ref. AYA2008-02948) and Application of the Satellite Radar Interferometry and the Global Navigation Satellite Systems to the control of distortions in the Baetic Cordillera (Ref. AYA2010-15501), funded by the Spanish government. The authors would like to thank Francisco Gonzalez for his contribution in the development of PCube, IGS for providing GPS observations and satellite products, ESA for providing GESS observations and GPC products, and the online PPP programs CSRS-PPP, magicGNSS, and APPS for their valuable services. We also appreciate the reviewers' suggestions and improvements to this manuscript.

References

Bisnath S, Gao Y (2007) Current state of precise point positioning and future prospects and limitations. In: Proceeding of IUGG 24th general assembly, 2–13 July 2007, Perugia, Italy

Crisci M, Hollreiser M, Falcone M, Colina M, Giraud J (2007) GIOVE mission sensor station performance characterization: overview of the results. In: Proceedings of the 20th international technical meeting of the satellite division of the institute of navigation (ION GNSS 2007), Fort Worth, TX, September 2007, pp 1028–1041

Dach U, Hugentobler U, Fridez R, Meindl P (2007) Bernese GPS software version 5.0. Astronomical Institute University of Bern

De Bakker PF, Tiberius C, van der Marel H, van Bree RJP (2012) Short and zero baseline analysis of GPS L1 C/A, L5Q, GIOVE

E1B, and E5aQ signals. GPS Solut 16(1):53–64. doi: 10.1007/s10291-011-0202-3

De Lacy C, Gil AJ, Rodriguez-Caderot G, Moreno B (2008) A method to estimate the ionospheric bias by using the new GNSS frequencies: an analysis of its theoretical accuracy in a PPP context. Física de la Tierra 20:133–150

Dow JM, Neilan RE, Rizos C (2009) The international GNSS service in a changing landscape of global navigation satellite systems. J Geod 83:191–198

Euler HJ, Goad CC (1991) On optimal filtering of GPS dual frequency observations without using orbit information. Bull Geod 65:130–143

Ge M, Gendt G, Rothacher M (2006) Integer ambiguity resolution for precise point positioning. In: Proceeding VI Hotine-Marussi symposium of theoretical and computational Geodesy

Ge M, Gendt G, Rothacher M, Shi C, Liu J (2008) Resolution of GPS carrier-phase ambiguities in precise point positioning (PPP) with daily observations. J Geod 82:389–399

Hopfield HS (1972) Tropospheric range error parameters: further studies. The Johns Hopkins University—Applied Physics Laboratory, Baltimore MD

ICD-GPS-200 (2000) Global positioning system wing (GPSW) systems engineering and integrations. Interface control document. IRN-200C-004

Juan JM, Hernández-Pajares M, Sanz J et al (2012) Enhanced precise point positioning for GNSS users. IEEE Trans Geos Rem Sen 50(10):4213–4222

Kouba J, Héroux P (2001) Precise point positioning using IGS orbit and clock products. GPS Solut 5(2):12–28

Moreno B, Radicella S, De Lacy C, Herráiz M, Rodríguez-Caderot G (2011) On the effects of the ionospheric disturbances on precise point positioning at equatorial latitudes. GPS Solut 15(4):381–390

Petit G, Luzum B (2010) IERS Technical note No. 36. Frankfurt am Main: Verlag des Bundesamts für Kartographie und Geodäsie, 2010. 179 pp. ISBN 3-89888-989-6

Píriz R, García AM, Tobías G et al (2008) GNSS interoperability: offset between reference time scales and timing biases BIPM and IOP publishing ltd. Metrologia 45:87–102

Saastamoinen J (1973) Contribution to the theory of atmospheric refraction. Bull Geod 105(1):279–298

Schoenemann E, Becker M, Springer T (2011) A new approach for GNSS Analysis in a multi-GNSS and multi-signal environment. J Geodetic Sci 1(3):204–214

Simsky A, Mertens D, Sleewaegen JM, Hollreiser M, Crisci M (2008) Experimental results for the multipath performance of Galileo signals transmitted by GIOVE-A satellite. Int J Navig Obs Article ID 416380. doi:10.1155/2008/41638

Tobías G, Hidalgo I, Mozo A et al (2009) Building Galileo navigation system: two years of GIOVE-M experimentation. In: Proceeding ION GNSS-2009, The Institute of Navigation, Savannah, Georgia, Sept, pp 2967–2979

Wu J, Wu C, Hajj G, Bertiger W, Lichtenr S (1993) Effects of antenna orientation on GPS carrier phase. Manuscripta Geodaetica 18:1647–1660

Zandbergen R, Navarro D (2006) Specification of Galileo and GIOVE space segment properties relevant for satellite laser ranging. Tech. Note, European Space Agency